

# Journal of Geophysical Research: Atmospheres

## RESEARCH ARTICLE

10.1002/2017JD027140

**Key Points:**

- High positive specific humidity (temperature) anomalies predominate for extreme WBT in hot/dry (cool/wet) climates
- The locations of the largest SST anomalies associated with extreme WBT vary by region and are primarily remote rather than local
- Moist low-level flows are the primary determinant of extreme-WBT location, timing, and intensity in many regions of the U.S.

**Supporting Information:**

- Supporting Information S1

**Correspondence to:**

C. Raymond,  
cr2630@columbia.edu

**Citation:**

Raymond, C., Singh, D., & Horton, R. M. (2017). Spatiotemporal patterns and synoptics of extreme wet-bulb temperature in the contiguous United States. *Journal of Geophysical Research: Atmospheres*, 122, 13,108–13,124.  
<https://doi.org/10.1002/2017JD027140>

Received 16 MAY 2017

Accepted 26 NOV 2017

Accepted article online 2 DEC 2017

Published online 19 DEC 2017

## Spatiotemporal Patterns and Synoptics of Extreme Wet-Bulb Temperature in the Contiguous United States

**C. Raymond<sup>1</sup> , D. Singh<sup>2,3</sup> , and R. M. Horton<sup>2,4,5</sup> **

<sup>1</sup>Department of Earth and Environmental Sciences, Columbia University, New York, NY, USA, <sup>2</sup>Lamont-Doherty Earth Observatory, Palisades, NY, USA, <sup>3</sup>School of the Environment, Washington State University, Vancouver, WA, USA, <sup>4</sup>Center for Climate Systems Research, Columbia University, New York, NY, USA, <sup>5</sup>NASA Goddard Institute for Space Studies, New York, NY, USA

**Abstract** Extremes of wet-bulb temperature (WBT)—jointly reflecting temperature and specific humidity—have seen relatively little study in terms of climatology, despite their demonstrated relevance for health and economic impacts. In this study, we uncover and characterize distinct spatiotemporal patterns of WBT extremes in the contiguous United States for the 1981–2015 period, focusing on identifying and making a first pass at understanding regional differences. We find that anomalies of specific humidity are of greater importance than those of temperature in controlling extreme WBT in most of the contiguous U.S., particularly for southern and arid regions. Composites of extreme-WBT days for each region reveal coherent sea-surface temperature anomalies and midlevel and upper -level geopotential-height anomalies that differ considerably between regions, particularly in terms of the resulting low-level temperature and moisture fields. These findings suggest that the primary factors controlling the timing and intensity of WBT extremes, while ultimately forced by synoptic-scale weather patterns, vary spatially according to both local geography and baseline climate. We demonstrate this conclusion by showing how regional features such as late-summer WBT extremes in the Southwest and southern Great Plains derive primarily from spatial and temporal variations in moist low-level flows.

**Plain Language Summary** Wet-bulb temperature (WBT), as a combination of temperature and humidity, is a good proxy for the health and economic impacts of heat. However, WBT extremes have rarely been studied. We assemble a new 35 -year hourly-resolution dataset from contiguous -U.S. weather stations. In the western U.S., we find that when the wind blows from a direction favorable for high temperature, it is simultaneously unfavorable for high humidity, but in the eastern U.S. extreme temperature and moisture are tightly linked. We devise a new approach to quantify the “moistness” of heat and find that WBT extremes often result from hot dry areas having unusual “moisture spikes,” or cool moist areas having “temperature spikes.” We show the first maps of the average time of year of WBT extremes—most interesting is the late-summer extreme WBT in the southern Great Plains and Southwest. We explain this in terms of moisture advection connected with the North American Monsoon (Southwest) and the strength of southerly winds from the Gulf of Mexico (Great Plains). Lastly, we find distinct atmospheric and sea surface temperature patterns associated with WBT extremes that differ between regions and that are present at least 10 days before the extremes, indicating the possibility of more accurate predictions.

### 1. Introduction

Many studies in the last few years have focused on extreme heat, in concert with a growing awareness of the diversity and severity of its impacts. As a result of these efforts, the overarching meteorology of extreme temperatures is now fairly well established. They are characterized to first order by the temporal and spatial cooccurrence of positive temperature and 500-hPa geopotential-height (z500) anomalies (Grotjahn et al., 2016; Lau & Nath, 2012; Perkins, 2015). In many cases, midlatitude extreme-temperature events can be attributed, in large part, to remote forcing by the excitation of Rossby waves from the tropics that propagate into the midlatitudes and become blocked over the affected region (Grotjahn et al., 2016). Atmosphere/land-surface coupling often aids in prolonging and exacerbating extreme-temperature events via soil-moisture and vegetation feedback (Grotjahn et al., 2016; Lorenz et al., 2010; Perkins, 2015). These factors have enabled demonstrations of subseasonal extreme-temperature predictability over parts of North America (McKinnon et al., 2016; Teng et al., 2013).

In contrast, the patterns and mechanisms of wet-bulb temperature (WBT) extremes have seen relatively little study. As the temperature to which an air parcel would cool if as much water as possible was evaporated into it, WBT is a nonlinear function of both temperature and specific humidity (Stull, 2011). WBT thus provides a good estimate of the cooling efficiency of sweat, and this direct physiological relevance has made it useful for assessments of heat stress. In fact, modeling studies have indicated that in some regions, WBT extremes could by the late 21st century verge on levels at which it is physiologically impossible to maintain normal human body temperatures (Im et al., 2017; Pal & Eltahir, 2016; Schär, 2016; Sherwood & Huber, 2010). A related and more complex quantity, wet-bulb globe temperature (WBGT), is frequently used in public-health research and to a lesser extent in climate science (Willett & Sherwood, 2012). Across metrics, heat-related morbidity and mortality increase sharply with increasing heat and humidity (Kalkstein & Davis, 1989; Willett & Sherwood, 2012), as do economic impacts (Dunne et al., 2013). These impacts would be nonlinear even in a stationary climate (Burke et al., 2015; Davis et al., 2016; Wu et al., 2014); adding to their importance is the fact that—in most observational records and all future projections—combined heat-humidity increases are more robust than increases in temperature or moisture alone (Fischer & Knutti, 2013; Grotjahn et al., 2016; Knutson & Poshay, 2016; Mora et al., 2017).

Changes in WBT can result from changes to either or both of its component variables, with specific humidity being less well constrained than temperature in models as well as observations. There has been some indication in recent observations that the high tail of the WBT distribution has seen tradeoffs between temperature and specific humidity in certain regions (Mueller et al., 2015; Willett & Sherwood, 2012) or over the course of a heat wave (Fischer et al., 2007). However, larger-scale studies have observed increases in temperature with constant relative humidity, and therefore higher WBT overall (Horton et al., 2016; Knutson & Poshay, 2016; Vincent et al., 2007; Willett & Sherwood, 2012).

Given these findings and motivations, we present here the first characterization of the patterns and synopses of WBT extremes across the contiguous United States, highlighting differences between regions. Our goal is to advance understanding of the mechanisms of WBT extremes, a step toward ultimately enabling skillful subseasonal forecasts. The paper is organized as follows: in section 2 we describe data sets, definitions, and methodology used. In section 3 we illustrate and discuss basic spatiotemporal patterns of WBT-extreme occurrence, and in section 4 of the interplay between temperature and specific humidity that underlie them. In section 5, we identify associated sea surface temperature, atmospheric circulation, and energy-flux anomalies at hemispheric and regional scales. Finally, in section 6 we integrate the pattern and mechanism sections into a preliminary but wide-ranging picture of WBT extremes in the contiguous U.S.

## 2. Methods

### 2.1. Data Sets

The station-selection procedure is as follows: using the National Climatic Data Center's Integrated Station Database, we choose contiguous U.S. stations with hourly data for all years in 1981–2015. For these 520 stations, we standardize irregularly timed observations using linear interpolation such that there is one observation each hour at the top of the hour, and conduct additional interpolation to fill data gaps of up to four consecutive hours. Then, we apply the following two criteria to eliminate station-year combinations: (a) having a data gap of  $\geq 4$  h or (b) having  $\geq 3\%$  of T or RH data missing. A station is eliminated completely if  $>33\%$  of its years have been disallowed. We enact additional quality control by algorithmically and visually identifying outliers, and comparing these with other values at the same station and nearby. The final version of the station data, composed of the 175 stations that passed all tests, is publicly available on Github (see Acknowledgments and Data Sources).

These 175 stations provide us with temperature (T), relative-humidity (RH), and surface-wind data at hourly resolution. From T and RH, we compute specific humidity (q) and WBT, the latter using the formula of Stull (2011):

$$\begin{aligned} \text{WBT} = & T \tan^{-1} \left[ 0.151977(RH + 8.313659)^{0.5} \right] + \tan^{-1}(T + RH) - \tan^{-1}(RH - 1.676331) \\ & + 0.00391838(RH)^{1.5} \tan^{-1}(0.023101RH) - 4.686035, \end{aligned}$$

where WBT and T are in  $^{\circ}\text{C}$  and RH is in %.

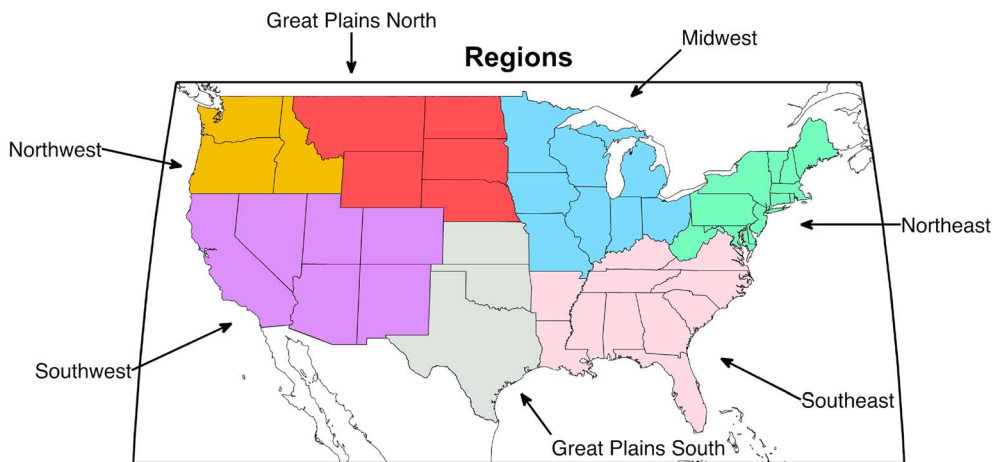


**Figure 1.** The seven regions used in this study. These are identical to those in the National Climate Assessment (Melillo et al., 2014) with the exception of the Great Plains, which we split into northern and southern sections.

Geopotential-height, winds, moisture, and energy-flux data come from the North American Regional Reanalysis (NARR) data set at 3-hourly and daily, 32 km resolution (Mesinger et al., 2006), as well as the National Centers for Environmental Prediction Reanalysis 2 data set at daily, 1° resolution (Kanamitsu et al., 2002). We use sea surface temperature (SST) data from the daily,  $0.25^\circ \times 0.25^\circ$  NOAA Optimum Interpolation SST data set (Reynolds et al., 2002), with results verified via comparison of the aggregated daily values with the monthly,  $2^\circ \times 2^\circ$  International Comprehensive Ocean-Atmosphere Data Set (Freeman et al., 2016).

## 2.2. Definition of Extremes and Regions

We choose WBT as the principal variable of interest, in accordance with previous work on heat-humidity extremes at regional and global scales (Im et al., 2017; Pal & Eltahir, 2016; Sherwood & Huber, 2010). We compute daily maxima for individual stations for T, q, and WBT, and these maxima can occur at any time of day. Regions (Figure 1) are based on those used in the National Climate Assessment (Melillo et al., 2014): Northwest (NW), Southwest (SW), Great Plains North (GPN), Great Plains South (GPS), Midwest (MW), Southeast (SE), and Northeast (NE). We then compute daily regional maxima by averaging values across all  $n$  stations within each region, with  $n$  ranging from 14 (NW) to 39 (SE). We also independently calculate extreme days for each grid cell in the NARR data set to provide more complete spatial coverage and to test whether it can successfully represent the patterns found in the station observations.

To determine the most-extreme days as ranked by T, q, and WBT, we compute (for each variable, at each station) the 100 highest daily maxima of that variable in the warm season (May–October (MJJASO)) for the period of 1981–2015. Subsequently, we use “extremes” to refer to these sets of the 100 highest daily maxima at a station or in a region. We choose MJJASO as the period in which nearly all WBT extremes occur in the contiguous U.S., and 100 as representing approximately the top 1.5% of all days in MJJASO, or an average of about 3 days per year. We consider consecutive extreme days independently, following the lead of McKinnon et al. (2016), who find that the final difference in circulation composites is small between heat waves and individual hot days.

## 2.3. Comparison of Temperature and Moisture

To disentangle temperature and moisture effects on extreme WBT, we first calculate anomalies of T and q at the exact hour of the daily-maximum WBT for the 100 extreme-WBT days at each station. These anomalies are computed relative to each station’s smoothed hour-specific climatology, where the smoothing is accomplished by fitting  $n = 4$  harmonics to the curve of averages for each calendar day. We then compute a standardized anomaly ratio (SAR):

$$\text{SAR} = \left[ \frac{(O_T - C_T)}{\sigma_T} \right] / \left[ \frac{(O_q - C_q)}{\sigma_q} \right]$$

where  $O$  is the observed value for each variable and  $C$  and  $\sigma$  are its climatological mean and standard deviation, respectively. (We note that working with a set of extremes means that the ratio nowhere goes to zero.) Repeating this calculation for the 100 highest extremes, we compute the median standardized anomaly ratio as

$$\text{MSA} = \text{median}\{\text{SAR}_1, \text{SAR}_2, \dots, \text{SAR}_{100}\}$$

Averaged across a region, the MSA ratio can be interpreted as the relative fraction of extreme WBT attributable to each variable in the different regions: a larger (smaller) MSA ratio implies that T (q) excursions are of relatively greater importance in controlling extreme WBT. In other words, the larger the MSA ratio for a region, the more anomalously hot and/or dry are the conditions associated with its WBT extremes. We use the MSA ratio to define the “T/q composition” of a set of WBT extremes as T-dominated (MSA ratio  $> 1$ ), neutral (MSA ratio  $\sim 1$ ), or q-dominated (MSA ratio  $< 1$ ). These terms are of course valuable mostly in a comparative sense, and we note that the value 1 is an arbitrary, though useful, reference point. We also acknowledge that the MSA-ratio approach has limitations, particularly in its reliance on many different local climatologies and in its lack of direct connection to any thermodynamic quantities; nonetheless, we feel that it has a heuristic value appropriate for the characterization of WBT patterns.

#### 2.4. Creation of Composites

To identify the circulation and surface conditions associated with regional WBT extremes, we create composites for these days of z500 and SST anomalies across the Northern Hemisphere, and of 850 hPa temperature, specific humidity, and wind anomalies across the contiguous U.S. Details about determining statistical significance for the SST-anomaly composites are provided in section S1 of the supporting information.

### 3. Basic Patterns

#### 3.1. Median Wet-Bulb Temperatures

Plotting the median of the 100 WBT extremes (i.e., the 50th highest) at each station (Figure 2), we find the highest values of 28–29°C in the SE and Mississippi Valley extending up to the lower MW, a geographic pattern also seen in earlier heat-wave and summer-mean studies of joint temperature-humidity extremes (Kalkstein & Valimont, 1986; Smith et al., 2013). The northward extent of these extremes around 90° W is likely associated with the climatological southerly flow of warm and moist air from the Gulf of Mexico (Figure 11h). Extreme-WBT values are also in excess of 25°C in the upper MW and coastal NE. These results quantitatively match previous work that found annual-maximum WBT of 25–28°C across much of the tropics and subtropics (Sherwood & Huber, 2010). Extreme WBT is significantly lower in the drier western half of the U.S., with the highest values there approximately equaling the lowest ones in the east. These patterns are also captured qualitatively by the NARR data set (Figure 2).

#### 3.2. Temporal Patterns of Variability

The mean date of extreme-WBT occurrence falls in midsummer in most of the country (Figure 3a), but in early summer in central Texas and in late summer in the desert SW and coastal California. Mean dates of extreme T (Figure 3b) follow a similar pattern but are reversed in the aforementioned areas, being mostly in midsummer except along the Gulf Coast (late summer) and the desert SW (early summer). For the SW, this matches previous work showing that T (WBT) extremes there typically occur prior to (following) the onset date of the North American Monsoon, a consequence of the low soil moisture, high insolation, and dry atmosphere in early summer (Higgins & Shi, 2000). Late-summer extreme T on the Gulf Coast may be related to the climatologically weaker southerly flow off of the Gulf of Mexico in August (Weaver et al., 2009), tending to cause increased continental influence and higher temperatures (Kalkstein & Valimont, 1986). The later date of extreme WBT (Figure 3a) as compared with extreme T (Figure 3b) more generally may be connected with the high heat capacity of the oceans and consequent peak in SSTs in late summer or early autumn, though more work is necessary on this issue.

The NARR data set provides support for these distinct regionally homogeneous patterns (Figure 3) and allows more detail to be seen in station-sparse areas. The set of independently identified extreme days

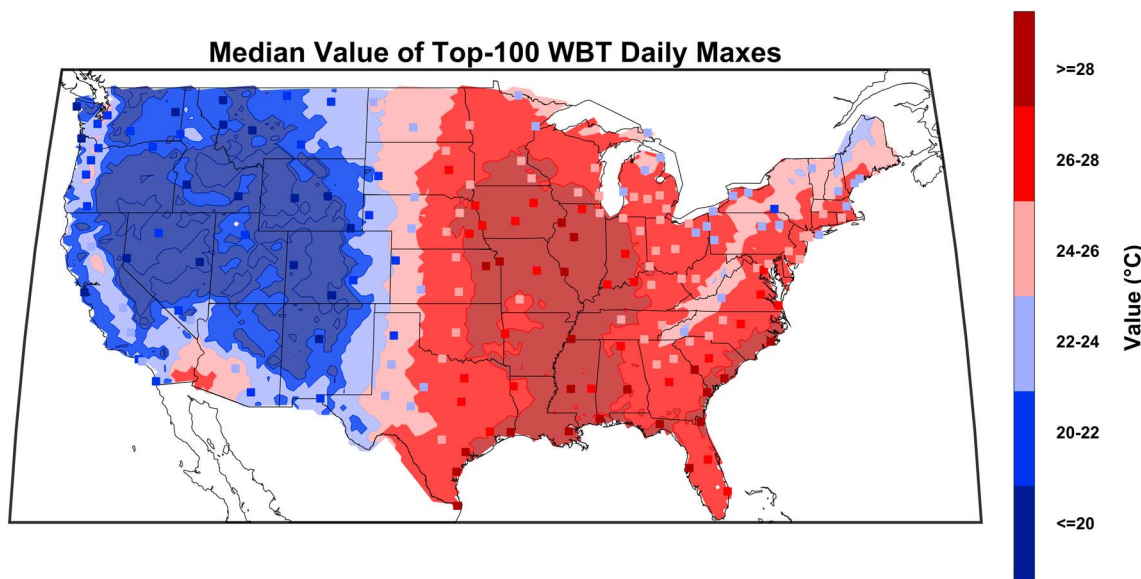


**Figure 2.** The median value of the 100 extreme-WBT daily maxima for each station (squares) and NARR grid cell (shading), computed using data from May–October of each year in 1981–2015.

at a NARR grid cell could differ substantially from the sets computed for nearby stations—due to coastal or elevation effects, temporal-resolution issues, or incomplete station spatial coverage—and a combination of these do cause some differences, particularly along the coasts and in parts of the SW. However, NARR and station data show good qualitative agreement overall, pointing to the robustness of the patterns and to NARR’s ability to reasonably represent the conditions under which surface WBT

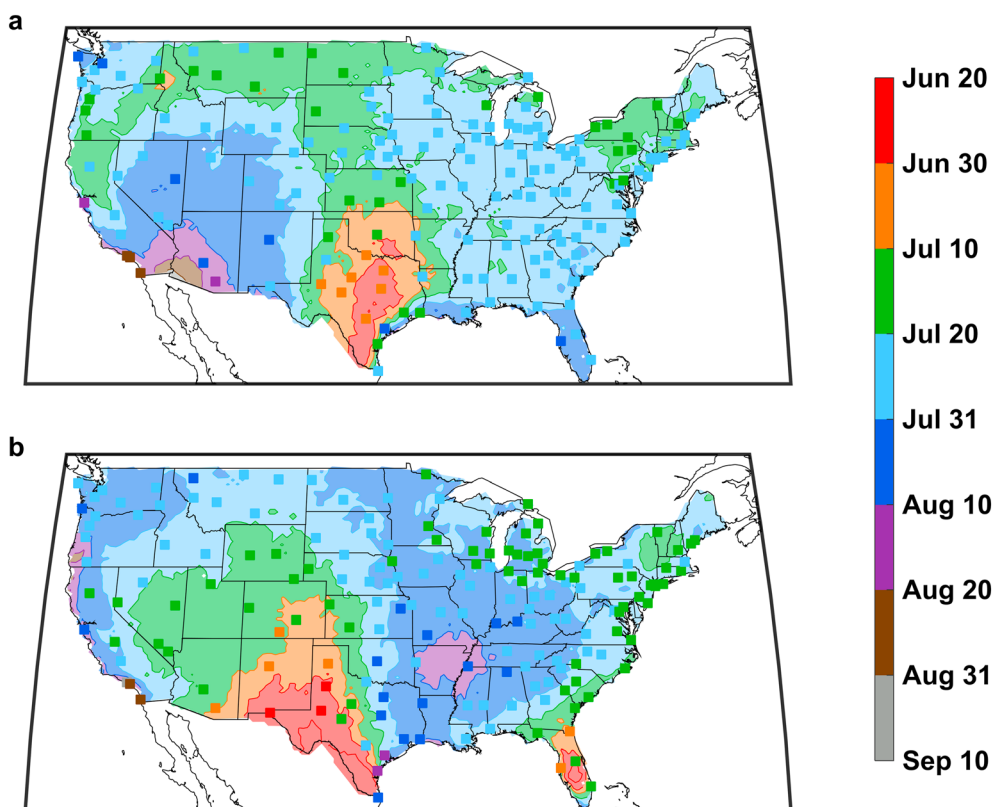


**Figure 3.** The mean calendar date of (a) the 100 extreme-WBT days and (b) the 100 extreme-T days for each station (squares) and NARR grid cell (shading).

### Average Hour of Occurrence of the 100 Highest Wet-Bulb Temperatures

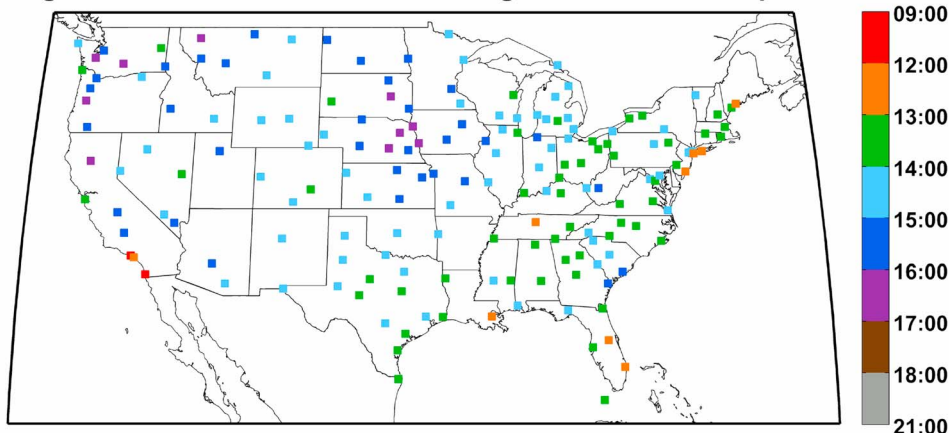


**Figure 4.** The mean hour of the day (LST) at which the 100 extreme-WBT daily maxima occur at each station.

extremes occur. Quantitatively, extreme-WBT values in NARR are often too low by several degrees K, consistent with a dry bias in the lower atmosphere that may be an artifact of its coarse temporal resolution (Kennedy et al., 2011).

At sub-daily timescales, extreme WBT occurs on average as early as 1200 local standard time (LST) at eastern and western coastal stations, and as late as 1700 LST in the MW, GPN, and interior NW (Figure 4). WBT extremes are typically later in the interior of the country, possibly due to the importance of  $q$  for WBT extremes there (Figure 5), making them less tied to the diurnal cycle than T-dominated extremes would be. Multiple mesoscale factors could also be at play, investigation of which is beyond the scope of this study.

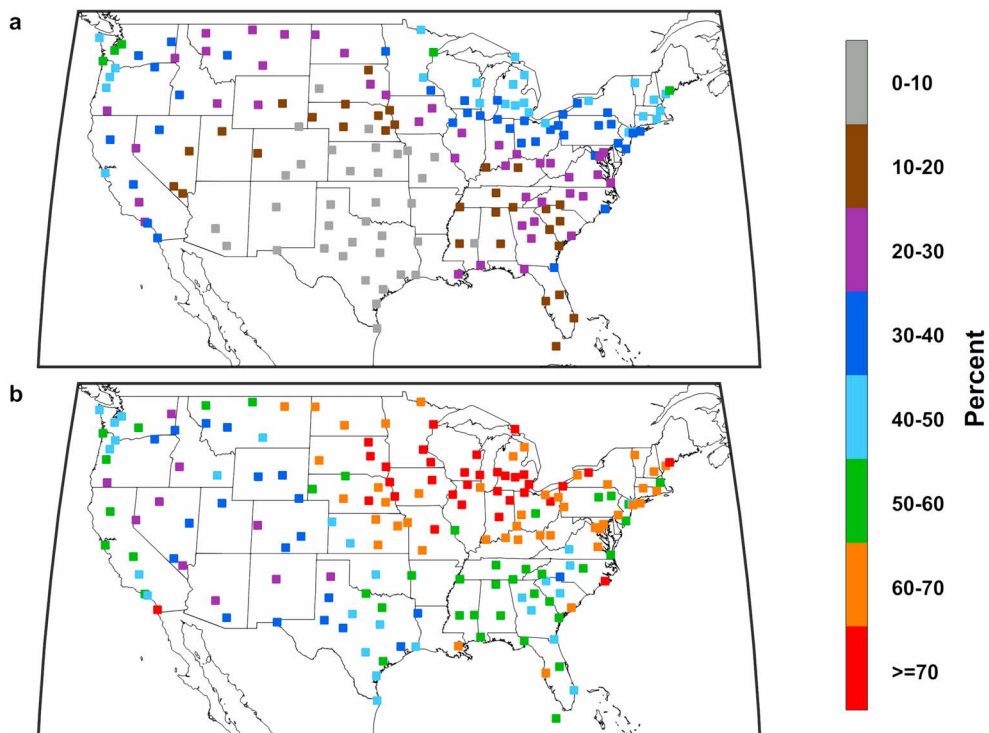


**Figure 5.** (top) The percent overlap between the 100 extreme-WBT days and the 100 extreme-T days at each station. (bottom) The same metric for WBT/q overlap.

## 4. Relative Contributions of Temperature and Moisture

### 4.1. Cooccurrence of Wet-Bulb-Temperature, Temperature, and Specific-Humidity Extremes

There have been some previous efforts to separate out the influence of atmospheric temperature and moisture (Pielke, Davey, & Morgan, 2004), but to our knowledge, no such analysis has been conducted across multiple regions or aimed at characterizing spatiotemporal variations in extreme WBT. To illustrate the spatially varying roles of  $q$  and  $T$  in driving WBT extremes, we compare the percent overlap between (1) days with WBT extremes and days with  $q$  extremes and (2) days with WBT extremes and days with  $T$  extremes (Figure 5). Whereas WBT and  $q$  extremes are frequently simultaneously observed in much of the eastern U.S. and parts of the western, WBT and  $T$  extremes generally coincide less than 30% of the time. This suggests that WBT extremes are primarily driven by conditions that lead to extreme  $q$ . The disjunct nature of  $T$  and WBT extremes is most pronounced in the semiarid GPS and SW, where  $T$ - $q$  overlap is also low. Greater  $T$ -WBT overlap is observed (1) near water bodies such as the Pacific Ocean, Atlantic Ocean, and Great Lakes and (2) further north at a given longitude.

### 4.2. Excursions of Temperature Versus Moisture

We apply the MSA-ratio approach (section 2.3) to examine more closely the spatial patterns described in section 4.1. Variations in the MSA ratio are spatially coherent, with the scarcity of reds in Figure 6 indicating that at times of extreme WBT,  $q$  is relatively more extreme than  $T$  over most of the country. In a stationary-climate framework, regions with especially high or low MSA ratios can be interpreted as reflecting empirical limitations on the range of  $T$  and  $q$  combinations: where  $q$  ( $T$ ) is climatologically high—especially in concert with  $T$  ( $q$ ) being low—a WBT extreme is most likely to occur through a large excursion of  $T$  ( $q$ ) (Figures 7a and 7b). This reasoning accounts for the larger MSA ratios along the cool and humid Pacific coast, in contrast to the smaller MSA ratios of the GPS and Great Basin (Figure 6). A Clausius-Clapeyron-based argument helps explain the  $q$  dominance of subtropical areas like Florida: the nonlinearity of WBT with respect to  $q$ , combined with the increasing moisture capacity of air at higher  $T$ , means that warmer areas are more likely to experience  $q$  dominance than cold ones where  $q$  is intrinsically limited. Consequently, along the East Coast we find stronger  $q$  dominance in the south, with more balance between  $T$  and  $q$  further north (Figure 6). Both arguments elucidate why a region's baseline climate is a strong predictor of the  $q$ -dominance of its WBT extremes (Figures 7c and 7d). The role of the atmospheric circulation may also be substantial, through its effect on variability, and future work could aim to identify and quantify this.

Comparing MSA ratios on seasonal timescales (Figure 8) yields insights about the causes, in a climatological sense, of variations in extreme WBT. Most regions show a tendency for shoulder-season WBT extremes to have larger standardized anomalies of  $T$  and  $q$ , likely a reflection of lower mean values. This is especially so for  $q$  extremes in the eastern U.S. (MW, NE, and SE; Figures 8e–8g), indicating an outsize role for moisture in driving WBT extremes at those times. Splitting the SW into coastal and desert subregions shows more clearly the influence of seasonal variations in local climate on the  $T/q$  composition of WBT extremes (Figure 9). Consistent with the discussion in the preceding paragraph, although early summer is typically cool and moist along the California coast, when WBT extremes do occur they are associated with greater  $T$  standardized anomalies than those that occur later in the summer (Figure 9)—probably because the principal mechanism (advection of hot, dry air from the interior) is the same but the early-summer climatology is cooler at the coast (Lee & Grotjahn, 2016). Conversely, in the North American Monsoon area of Arizona and New Mexico, the MSA ratio becomes progressively smaller as neutral  $T/q$  composition in June yields to moisture surges that tend to cap temperatures in mid-to-late summer (Figure 9) (Adams & Comrie, 1997); see further discussion in section 5.3. Water vapor's effects on soil moisture (via precipitation) are likely an additional mechanism, but one we do not explicitly investigate here.

## 5. Circulation Anomalies and Regional Synopsics

### 5.1. Sea-Surface Temperature

Nearly every region has considerable areas of significant remote positive SST anomalies that are of larger magnitude than the anomalies nearest to it, though a few regions (NW, SW, and NE) do have significant nearshore SST anomalies (Figure 10). These nearshore anomalies could have an important role in modulating WBT extremes on interannual timescales. The SST anomalies for eastern-U.S. WBT extremes (Figures 10e–10g)

### Ratio of Median Standardized Anomalies of T and q at Hours of Extreme WBT

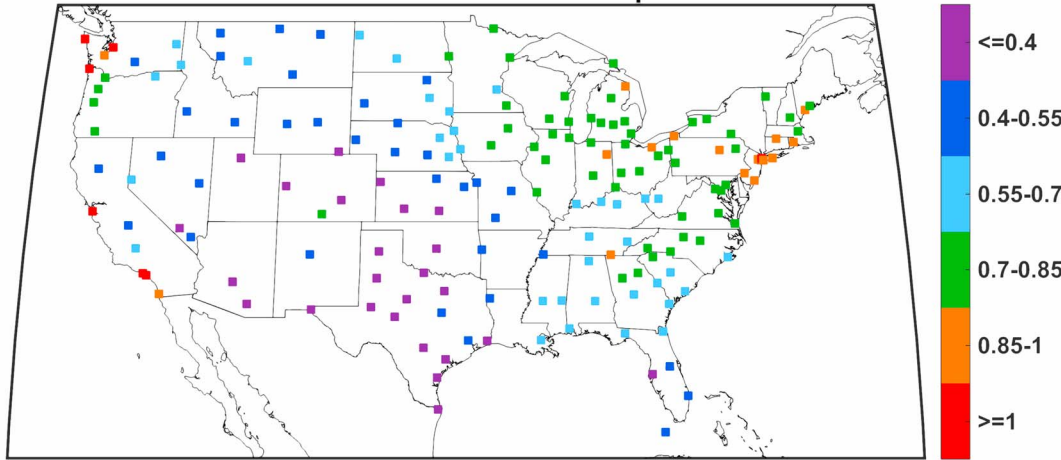


**Figure 6.** The median-standardized-anomaly ratio (see section 2.3 for description) computed using the 100 extreme-WBT daily maxima at each station, with purple indicating stations where WBT extremes are dominated by q excursions.

closely match in position and magnitude the “Pacific Extreme Pattern” for T extremes described in McKinnon et al. (2016), as well as elsewhere (Perkins, 2015; Teng et al., 2013; Loikith & Broccoli, 2012). For the NW and SW, the SST correlations resemble a PDO-like pattern with negative anomalies across the North Pacific (Mantua & Hare, 2002), suggesting some degree of potential region-specific decadal-scale modulation. In contrast, the GPN and GPS exhibit shorter-wavelength SST signatures in the north-central Pacific

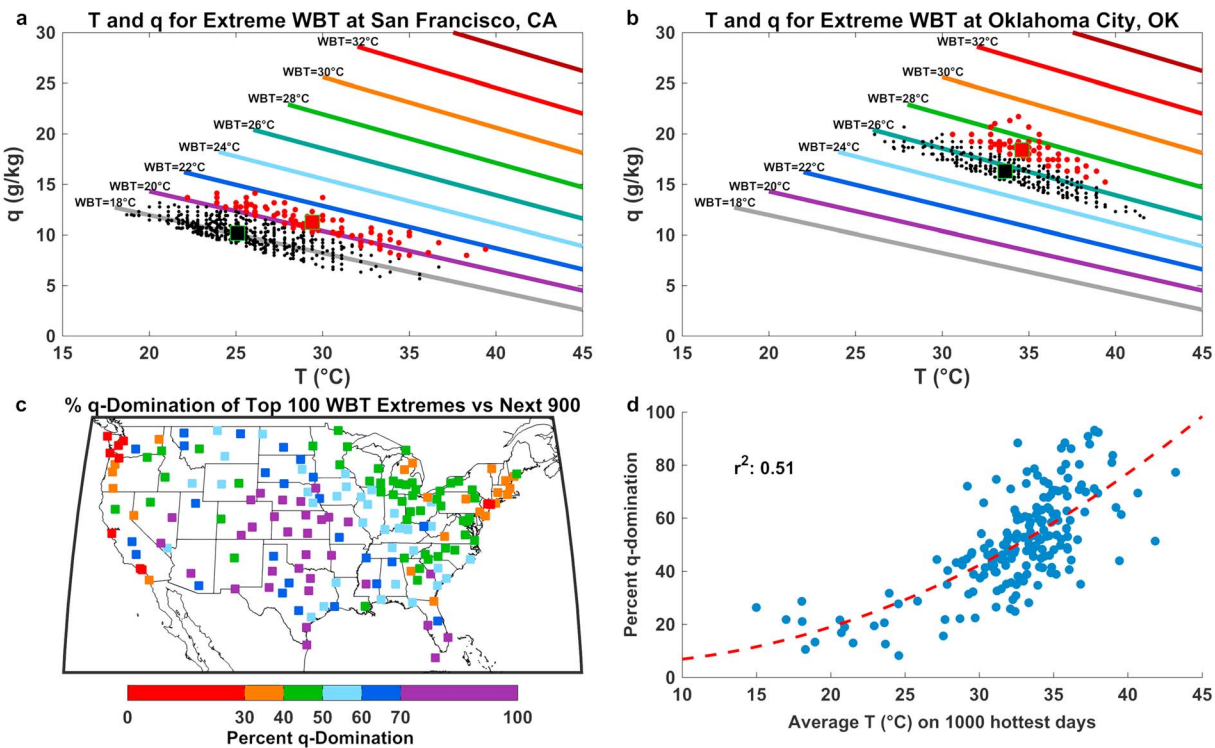


**Figure 7.** An illustration of the definition of (a) T-dominated and (b) q-dominated WBT extremes, where the red (black) dots represent WBT extremes #1–100 (#101–1000), plotted in T-q space for San Francisco, CA, and Oklahoma City, OK. The large squares within the clouds of dots (outlined in light green) are the mean of each set, and the superimposed colored lines are constant values of WBT. The more vertical the vector from the black square to the red square, the more q-dominated are a station’s WBT extremes. Due to finite instrument precision, some values may be identical to others and therefore plot directly on top of them. (c) The percent q-dominance for each of the 175 stations, computed using the angle of the vector between the large black dot and the large red dot for each station (as in Figures 7a and 7b), which is converted to a q-dominance percentage where  $0^\circ \rightarrow 0\%$  and  $90^\circ \rightarrow 100\%$ . (d) The percent q dominance for each station, as in Figure 7c, plotted against the mean daily maximum temperature on its 1000 hottest days in the 1981–2015 period.

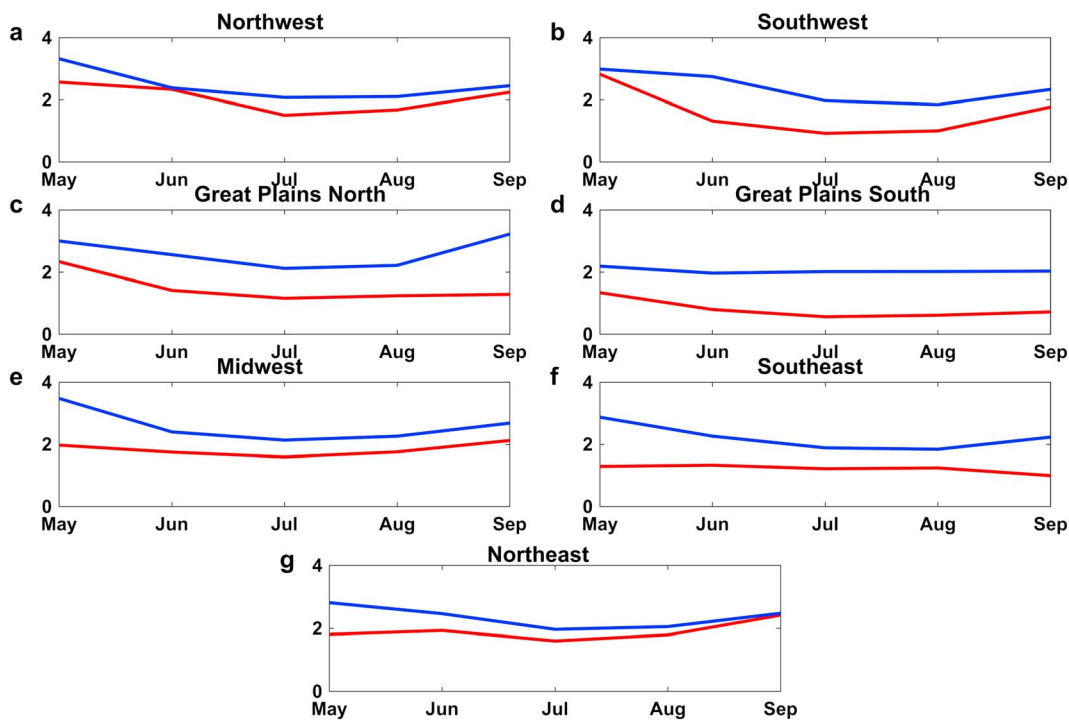


**Figure 8.** The red (blue) lines represent the regional means of the median standardized anomaly of T (q) at the time of WBT extremes in each warm-season month, averaged across the 100 WBT extremes of all the stations in a region.

(Figures 10c and 10d); for the GPS, there is also a statistically significant connection with the El Niño–Southern Oscillation, resembling a La Niña-like phase (Figure 10d). These patterns and correlations deserve further attention to help inform predictability.

### 5.2. Upper Level Flow

The z500 anomalies for each region’s extreme-WBT days consist of a positive anomaly centered near or directly over that region, with weaker negative anomalies immediately upstream and downstream

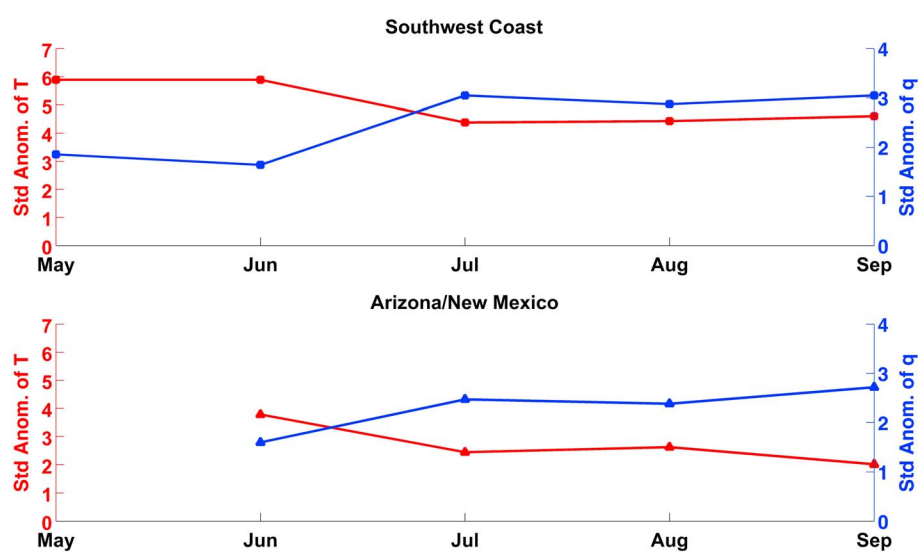


**Figure 9.** The seasonal evolution of the T (red) and q (blue) standardized anomalies associated with WBT extremes, averaged across the  $n = 4$  stations in the (top) coastal Southwest and the  $n = 3$  stations in (bottom) Arizona and New Mexico. Note that the latter set of stations had no May WBT extremes in any year. Unlike in previous figures, standardized anomalies are here computed for each station relative to the entire MJJASO period, so that values for different months can be directly compared.

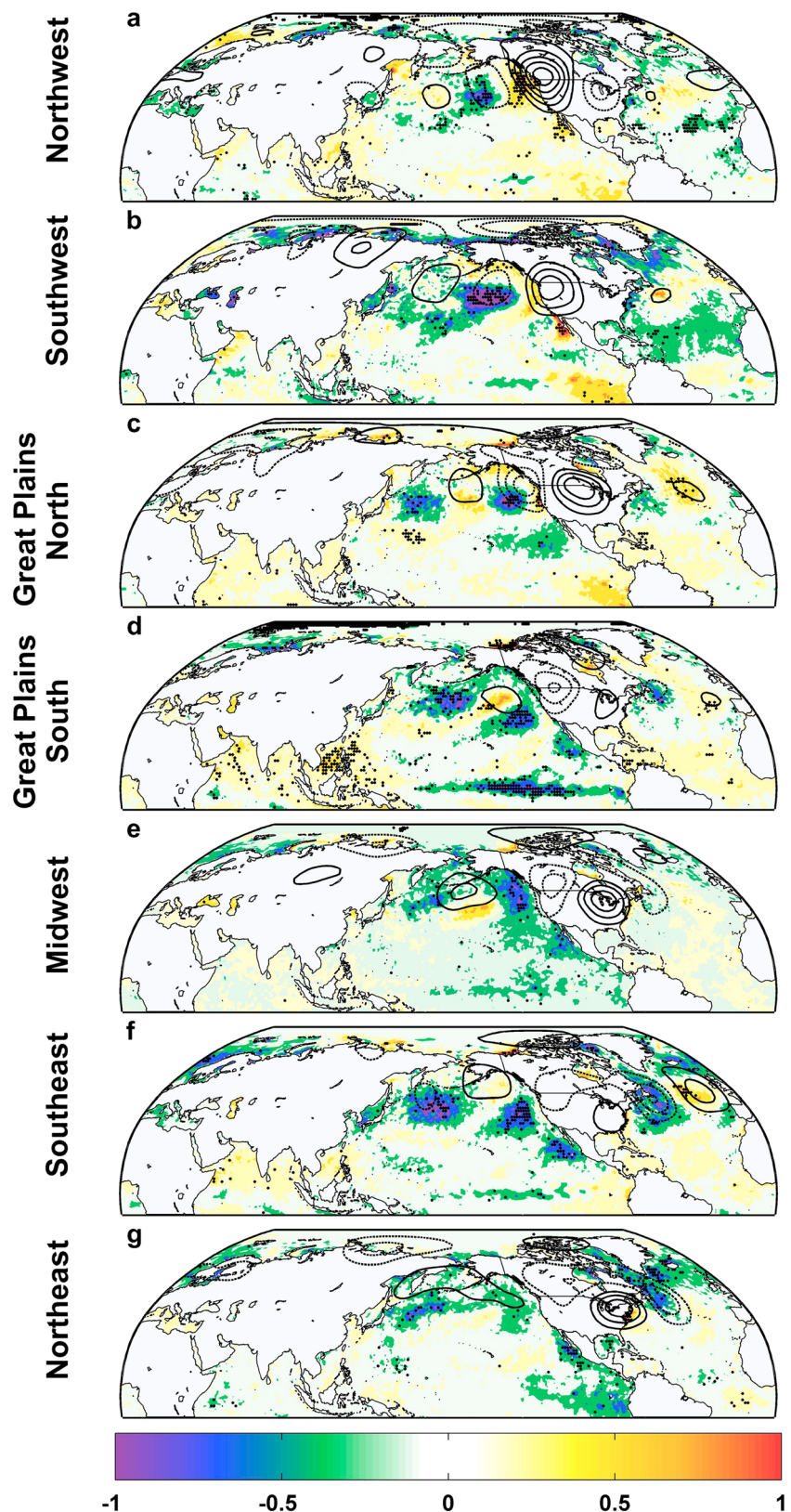


**Figure 10.** Composites of the daily z500 anomalies (contours, at 20 m intervals, with negative dashed and zero omitted) and SST anomalies (shading, stippled at 95% significance) on the 100 extreme-WBT days in each region. The colorbar represents the SST anomaly, in units of °C.

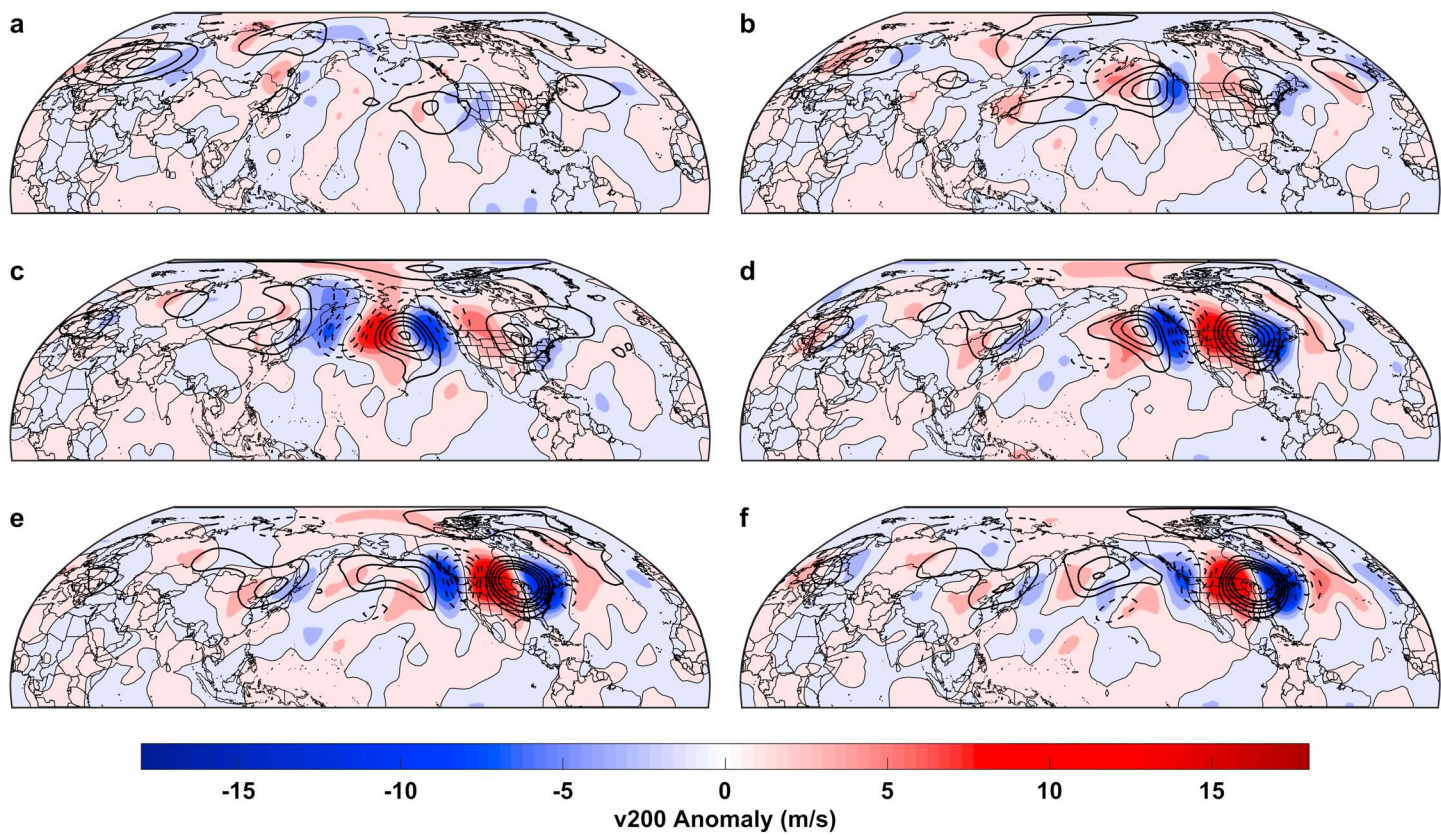


**Figure 11.** Composites of daily anomalies of 200 hPa geopotential height (contours, at 20 m intervals, with negative dashed and zero omitted) and 200 hPa meridional wind (shading) in the period leading up to the 100 extreme-WBT days in the Midwest: (a) 20 days prior; (b) 10 days prior; (c) 5 days prior; (d) 2 days prior; (e) 1 day prior; (f) the extreme-WBT day. Preceding days with an intervening WBT extreme were excluded.

(Figure 10). To further investigate the nature of the upper-level waves, in Figure 11 we plot a time series of anomalies of 200-hPa meridional winds ( $v_{200}$ ) and geopotential heights ( $z_{200}$ ) for MW WBT extremes, on the model of Teng and Branstator (2017). The developing ridge over the MW is apparent by 10 days prior to the extreme (Figure 11b), in terms of both  $z_{200}$  and  $v_{200}$ . The  $v_{200}$  anomalies indicate origination of the wave-train in the midlatitudes of eastern Asia and subsequent propagation across the Pacific, a path very similar to that found by Teng and Branstator (2017).

### 5.3. Low-Level Flow

WBT extremes in the eastern and central U.S. are characterized by a westward-expanded Bermuda High and strong southerly flow over the middle of the country, also noted in case studies of the March 2012 and July–August 1988 heat waves (Figures 10e–10g, 11f, and 12e–12g) (Dole et al., 2014; Trenberth & Guillemot, 1996). As a consequence, anomalous moisture builds into the MW and NE (Figures 12e–12g and 13e–13g), causing these WBT extremes to be closely associated with anomalous west-southwesterly winds over the Ohio Valley and large positive  $q$  anomalies from the MW to the Atlantic coast (Figures 12e–12g). This picture explains why extreme WBT and extreme T in the eastern U.S. are closely correlated (Figure 5b), and why the  $z_{500}$  and wind anomalies we find for extreme WBT are similar to those for extreme T (Cassano et al., 2006; Gershunov et al., 2009; Grotjahn et al., 2016; Kunkel et al., 1996; Lau & Nath, 2012; McKinnon et al., 2016; Teng et al., 2016).

For SW extreme-WBT days, a notable geographic separation exists between the locations of the maximum T anomalies (from central California to Montana; Figure 13b) and the maximum  $q$  anomalies (southern California, Nevada, and Arizona; Figure 12b). To investigate this further, we compute daily energy-flux anomalies of seven standard NARR variables (upward and downward shortwave and longwave radiations and ground, sensible, and latent heat), as well as of T and  $q$  advection using T and  $q$  at 2 m above ground level and wind speed at 10 m. T and  $q$  advection are converted to energy fluxes via the following formulae:

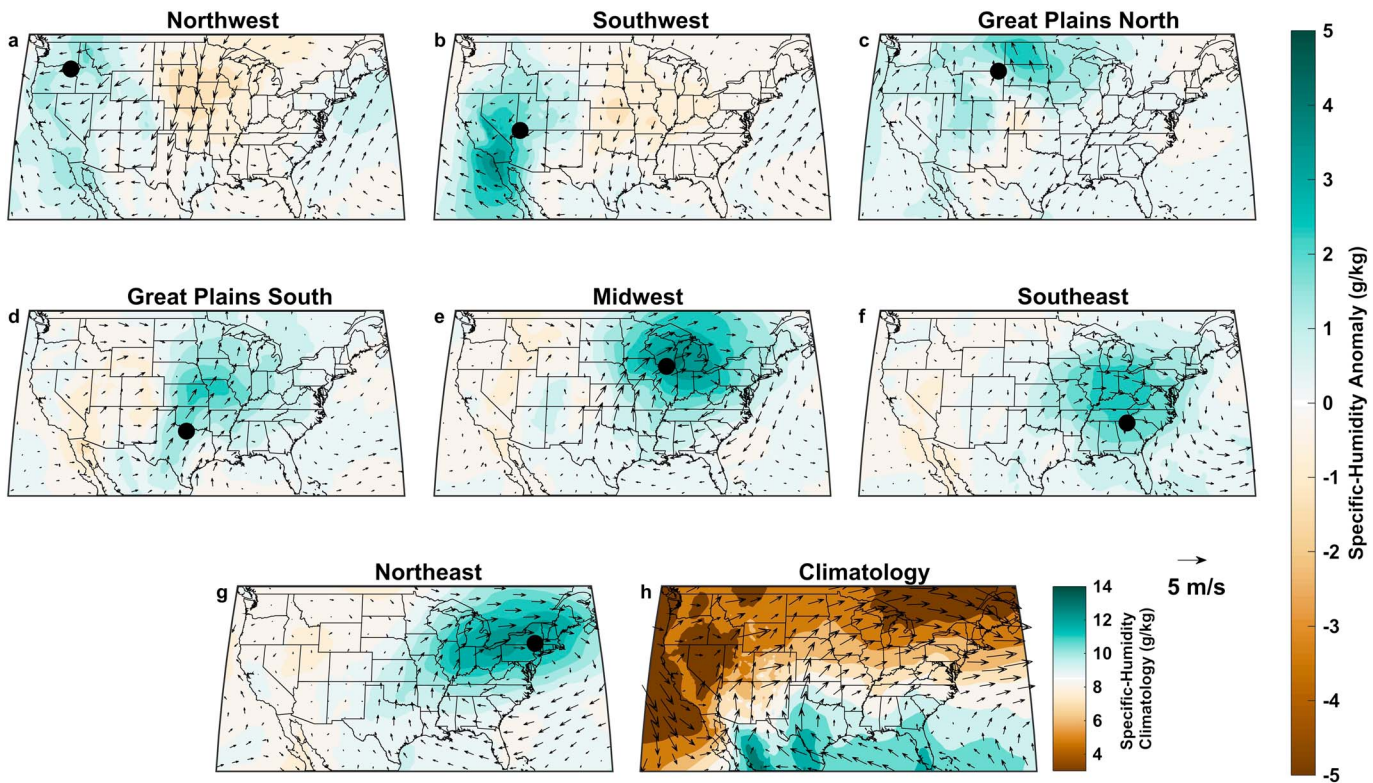


**Figure 12.** (a–g) Daily anomalies of 850 hPa specific humidity (shading) and 850-hPa wind (vectors) from the NARR data set for the 100 extreme-WBT days in each region. (h) Climatological 850 hPa specific humidity and wind for JJA.

$$T \text{ adv}_{W/m^2} = T \text{ adv}_{K/sec} * c_p * ACD$$

$$q \text{ adv}_{W/m^2} = q \text{ adv}_{(g/kg)/sec} * L * ACD$$

where  $c_p$  is the specific heat capacity of air at 300 K in  $J \text{ kg}^{-1} \text{ K}^{-1}$ , ACD is the mean atmospheric column density in  $\text{kg m}^{-2}$ , and  $L$  is the latent heat of vaporization of water in  $J/\text{g}$ . These conversions are our own, though comparisons between horizontally and vertically oriented energy fluxes have been made previously (Miralles et al., 2014; Trenberth et al., 2011; Nakamura & Oort, 1988). A clear temporal evolution of the anomalies is observed, with net positive flux peaking in the period of 2–4 days prior to extreme-WBT days in the SW (Figure 14). This net flux is largely driven by an increase in anomalous positive  $q$  advection, and secondarily by  $T$  advection; these drop to near average by the day after the most extreme WBT is observed. We conclude that  $q$  advection in the interior SW is important for causing  $q$  anomalies and thereby controlling extreme WBT there; this reveals the physical cause for the distinction between extreme-T and extreme-WBT days in the region (Figure 5b), and may be a signature of moisture pulses in connection with the North American Monsoon (Maddox et al., 1995). Given this distinction, it is to be expected that this synoptic picture stands in contrast to that for extreme  $T$  in California (Lee & Grotjahn, 2016).

In the NW, we highlight the role of local geography. An anomalous easterly wind (Figure 12a) prevents marine cooling due to the climatologically positive west-to-east  $T$  gradient (Figure 13h). On the western slope of the Cascades, adiabatic descent likely provides a further anomalous boost to  $T$  (Bumbaco et al., 2013). This picture is consistent with a comparable role for  $T$  and  $q$  anomalies in extreme-WBT days in the coastal NW (Figure 6).

The GPS also shows a geographic influence on the mechanism of its WBT anomalies. Maximum  $T$  anomalies are displaced to the northeast of the region, as are maximum z500 anomalies (Figure 13d), resulting in a low-level flow directly from the Gulf of Mexico (Figure 12d) rather than interior Mexico (as would be the case if the maximum anomalies were further west, centered over the region). That the GPS experiences almost no concurrent WBT and  $T$  extremes (Figure 5d) suggests that this moisture infusion is a necessary condition for extreme WBT there.

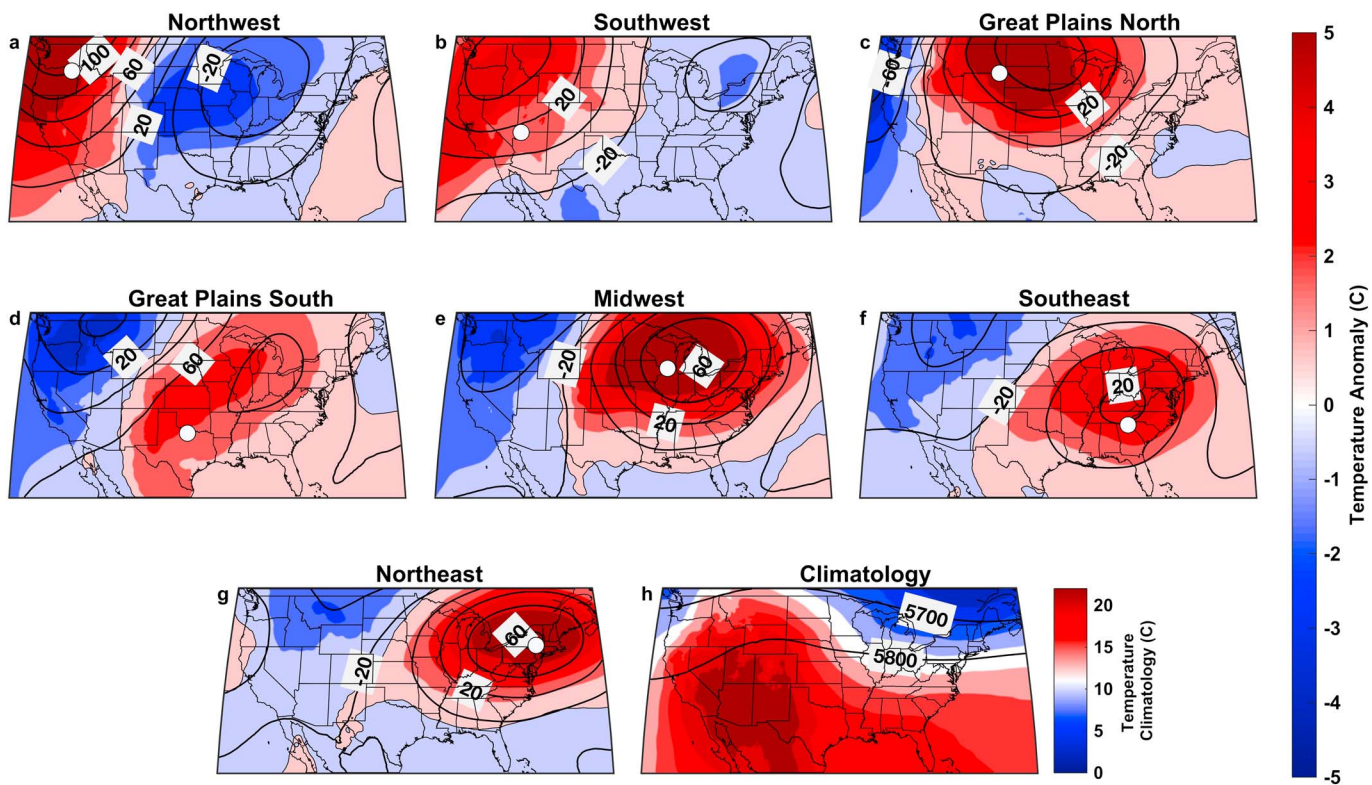


**Figure 13.** (a–g) Daily anomalies of 850 hPa temperature (shading; units of  $^{\circ}\text{C}$ ) and 500 hPa geopotential height (contours; units of m) from the NARR data set for the 100 extreme-WBT days in each region. (h) Climatological 850 hPa temperature and 500 hPa geopotential height for JJA.

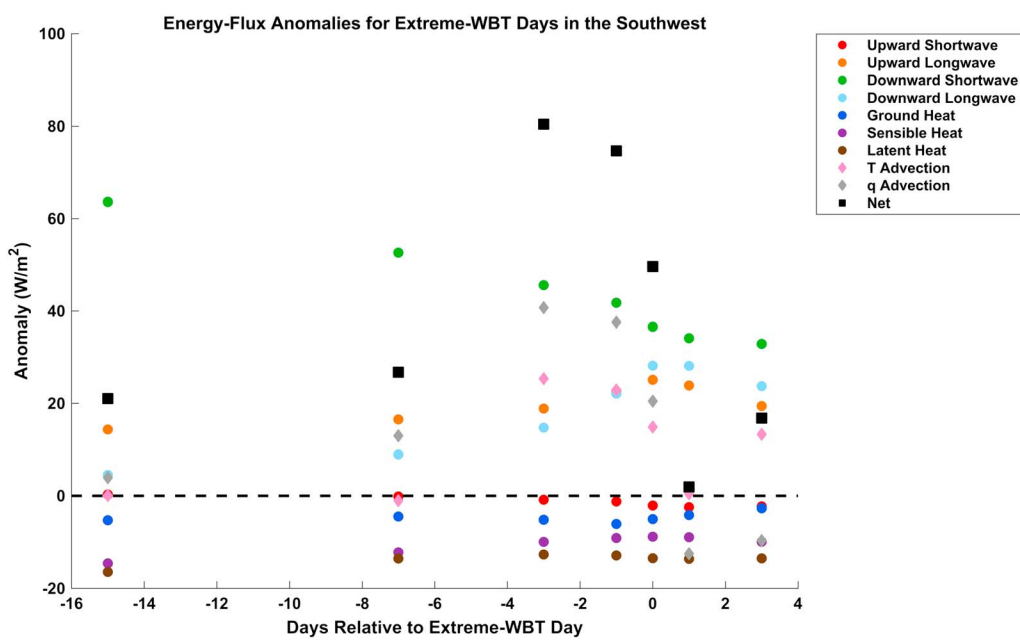


**Figure 14.** Surface energy-flux anomalies calculated from NARR data for SW extreme-WBT days, averaged spatially over the SW and temporally over the periods (from left): 20–10 days before the extreme, 9–5 days before, 4–2 days before, 1 day before, the extreme day, 1 day after, and 2–4 days after. The conversion of T and q advection to fluxes in  $\text{W/m}^2$  is described in section 5.3 of the text.

## 6. Discussion

The relationship we find between WBT extremes and various remote midlatitude SST anomalies (Figure 10) provides further evidence supporting the connection between midlatitude heat extremes and remote SSTs more generally (Feudale & Shukla, 2011a; McKinnon et al., 2016; Ning et al., 2015). While Hoskins and Karoly (1981) detailed the Rossby-wave response to tropical and subtropical forcing, we find such links only for the GPS (Figure 10d). This accords with the observation of McKinnon et al. (2016) of limited evidence for a link between daily tropical SSTs and extreme-T days in the eastern U.S. In our interpretation, this conclusion is also compatible with the picture painted by Sherwood and Huber (2010), who found a close linkage between global-average WBT extremes and tropical surface temperature, but at annual and multiannual timescales.

SST anomalies for the NW and SW (SE and NE) bear some similarity in wavelength and phasing to z500 anomalies in the Pacific (Atlantic) Ocean (Figure 10), a possible indicator of a “reinforcing” role for SST with respect to extreme WBT, as has been shown for extreme T (Feudale & Shukla, 2011b; Hartmann, 2015; Wang & Schubert, 2014). We expect that this may prove a fruitful area of future work, drawing on atmosphere-ocean coupled modeling especially.

The small or absent correlation between WBT extremes and nearshore SST anomalies for most regions with coasts (Figure 10) could be taken as suggestive that the strong local WBT effects of anomalous SST found in the Persian Gulf region by Pal and Eltahir (2016), if present in the contiguous U.S., are restricted to the immediate coast such that they are minimal in our regional averages. If so, the Pal and Eltahir (2016) result may be unique to the Persian Gulf region or confined to hot regions with strongly stratified seas. Any direct comparison, however, is obscured by the difference in timescale of analysis between this study—examining historical interannual variability—and the long-term-mean-change approach of Pal and Eltahir (2016). Regardless, the existence of a clear correlation in the NW and SW between extreme WBT and nearby SSTs (Figures 10a and 10b) is a novel result, and one whose mechanisms and consequences deserve additional investigation across a variety of timescales.

In devising the MSA ratio and using it to characterize the relative contributions of T and q in driving WBT extremes in different regions, we find q excursions to be more important than T excursions in most regions (“q dominance”) (Figure 6), with the degree of this dominance being determined largely by the climatological aridity/moistness of a given region. The overall larger role of q in determining extreme WBT is underscored by the significantly higher extreme-WBT values in the eastern U.S. (Figure 2). In the MSA ratio we hope to have created a metric useful for future work; we emphasize, however, that it is but one approach of many to characterizing WBT extremes. Another is the direct comparison of T and q anomalies as shown in Figure 7c, which yields very similar results, as is apparent by comparing Figures 6 and 7c.

Our findings with regard to the MSA ratio also have possible implications for the effect of climate change on extreme WBT. Both mean and extreme T and q are projected to increase over most of the globe, though with q increases likely falling behind an exact Clausius-Clapeyron scaling over land due to enhanced continental warming relative to oceanic (Held & Soden, 2006; Laîné et al., 2014; Wuebbles et al., 2015). Consequently, considerable extreme-WBT increases are expected almost everywhere, by an amount dependent both on the regional increase of T versus q and on the regional sensitivity of extreme WBT to T and q variation (as illustrated by the MSA ratio). If—as the weaker-vertical-circulation theory (Held & Soden, 2006), the q dominance of the hottest regions of the U.S. (Figure 6), and the greater non-linearity of WBT with respect to q than to T (Stull, 2011) all suggest—q indeed plays an ever-greater role in determining WBT at the higher temperatures of the future, we would expect to see q-dominance spread poleward. Jones et al. (2010) make an analogous postulation that moisture will play an increasing role in controlling extreme precipitation, and this double impact of moisture could be further explored, particularly regarding the possibility of far-right-tail WBT values beyond any observations to date (Pal & Eltahir, 2016; Sherwood & Huber, 2010).

## 7. Conclusions

In this paper we use the highest-quality available data to provide the first comprehensive characterization of the climatology and meteorology of WBT extremes in the contiguous U.S. We find regionally coherent

spatiotemporal patterns of extreme-WBT magnitude, timing, and T/q composition, many of which are closely linked to the local geography and climatology of each region. The underlying theme is the importance of specific humidity in determining WBT extremes in most regions, though there are areas (climatologically cool and moist ones) where temperature plays a role equally large or even larger. We also examine antecedent z500 and z200 wavetrains, which are apparent across the Pacific and North America for many regions, and cooccurring SST anomalies, which exhibit significant correlations even in remote locations. Together, these suggest the potential for region-specific predictability.

An examination of the energy fluxes surrounding WBT extremes in the Southwest reveals an increase in both T and q advection of  $\sim 40 \text{ W/m}^2$  several days before the event, and an especially large amount of q advection, in accord with the large q anomalies observed at the same time. More detailed region- and subregion-specific analyses of the patterns we have identified could aim to determine the exact dynamical and thermodynamical mechanisms responsible, their timing and interactions, their variations between events, and the scales over which they operate. Both modeling and observational analysis would help in elucidating these aspects of WBT extremes. Investigating other potential finer-scale controls on extreme WBT—e.g., strongly convective environments, sea breezes, and seasonal low-level jets—as well as the dynamical effect of SSTs and soil moisture would provide insights for improving our understanding of the multiscale drivers of WBT extremes in different climatic regimes.

#### Acknowledgments

The authors declare no conflicts of interest with regard to this research. Funding for R. Horton and C. Raymond was provided by the National Oceanic and Atmospheric Administration's Regional Integrated Sciences and Assessments program, grant NA15OAR4310147. C. Raymond also acknowledges support from the Columbia University Department of Earth and Environmental Sciences and the Columbia Climate Center. D. Singh received support from the Lamont-Doherty Earth Observatory Fellowship. Data supporting our findings can be obtained from the sources mentioned in section 3. Our final quality-controlled data set, containing the station observations on which much of the analysis was performed, is freely available on Github at <https://github.com/cr2630git/finalhourlystationdataset>.

#### References

- Adams, D. K., & Comrie, A. C. (1997). The North American Monsoon. *Bulletin of the American Meteorological Society*, 78(10), 2197–2213. [https://doi.org/10.1175/1520-0477\(1997\)078%3C2197:TNAM%3E2.0.CO;2](https://doi.org/10.1175/1520-0477(1997)078%3C2197:TNAM%3E2.0.CO;2)
- Bumbaco, K. A., Dello, K. D., & Bond, N. A. (2013). History of Pacific Northwest heat waves: Synoptic pattern and trends. *Journal of Applied Meteorology and Climatology*, 52(7), 1618–1631. <https://doi.org/10.1175/jamc-d-12-094.1>
- Burke, M., Hsiang, S. M., & Miguel, E. (2015). Global non-linear effect of temperature on economic production. *Nature*, 527(7577), 235–239. <https://doi.org/10.1038/nature15725>
- Cassano, E. N., Lynch, A. H., Cassano, J. J., & Koslow, M. R. (2006). Classification of synoptic patterns in the western Arctic associated with extreme events at Barrow, Alaska. *Climate Research*, 30, 83–97. <https://doi.org/10.3354/cr030083>
- Davis, R. E., McGregor, G. R., & Enfield, K. B. (2016). Humidity: A review and primer on atmospheric moisture and human health. *Environmental Research*, 144(Pt A), 106–116. <https://doi.org/10.1016/j.envres.2015.10.014>
- Dole, R., Hoerling, M., Kumar, A., Eischeid, J., Perlitz, J., Quan, X.-W., ... Zhang, T. (2014). The making of an extreme event: Putting the pieces together. *Bulletin of the American Meteorological Society*, 95(3), 427–440. <https://doi.org/10.1175/bams-d-12-00069.1>
- Dunne, J. P., Stouffer, R. J., & John, J. G. (2013). Reductions in labour capacity from heat stress under climate warming. *Nature Climate Change*, 3, 563–566. <https://doi.org/10.1038/nclimate1827>
- Feudale, L., & Shukla, J. (2011a). Influence of sea surface temperature on the European heat wave of 2003 summer. Part I: An observational study. *Climate Dynamics*, 36(9–10), 1691–1703. <https://doi.org/10.1007/s00382-010-0788-0>
- Feudale, L., & Shukla, J. (2011b). Influence of sea surface temperature on the European heat wave of 2003 summer. Part II: A modeling study. *Climate Dynamics*, 36(9–10), 1705–1715. <https://doi.org/10.1007/s00382-010-0789-z>
- Fischer, E. M., & Knutti, R. (2013). Robust projections of combined humidity and temperature extremes. *Nature Climate Change*, 3(2), 126–130. <https://doi.org/10.1038/nclimate1682>
- Fischer, E. M., Seneviratne, S. I., Vidale, P. L., Lüthi, D., & Schär, C. (2007). Soil moisture-atmosphere interactions during the 2003 European summer heat wave. *Journal of Climate*, 20(20), 5081–5099. <https://doi.org/10.1175/jcli4288.1>
- Freeman, E., Woodruff, S. D., Worley, S. J., Lubker, S. J., Kent, E. C., Angel, W. E., ... Smith, S. R. (2016). ICOADS release 3.0: A major update to the historical marine climate record. *International Journal of Climatology*, 37(5), 2211–2232. <https://doi.org/10.1002/joc.4775>
- Gershunov, A., Cayan, D. R., & Iacobellis, S. F. (2009). The great 2006 heat wave over California and Nevada: Signal of an increasing trend. *Journal of Climate*, 22(23), 6181–6203. <https://doi.org/10.1175/2009jcli2465.1>
- Grotjahn, R., Black, R., Leung, R., Wehner, M. F., Barlow, M., Bosilovich, M., ... Prabhat (2016). North American extreme temperature events and related large-scale meteorological patterns: A review of statistical methods, dynamics, modeling, and trends. *Climate Dynamics*, 46(3–4), 1151–1184. <https://doi.org/10.1007/s00382-015-2638-6>
- Hartmann, D. L. (2015). Pacific sea surface temperature and the winter of 2014. *Geophysical Research Letters*, 42, 1894–1902. <https://doi.org/10.1002/2015GL063083>
- Held, I. M., & Soden, B. J. (2006). Robust responses of the hydrological cycle to global warming. *Journal of Climate*, 19(21), 5686–5699. <https://doi.org/10.1175/jcli3990.1>
- Higgins, R. W., & Shi, W. (2000). Dominant factors responsible for interannual variability of the summer monsoon in the southwestern United States. *Journal of Climate*, 13(4), 759–776. [https://doi.org/10.1175/1520-0442\(2000\)013%3C0759:DFRFIV%3E2.0.CO;2](https://doi.org/10.1175/1520-0442(2000)013%3C0759:DFRFIV%3E2.0.CO;2)
- Horton, R., Mankin, J. S., Lesk, C., Coffel, E., & Raymond, C. (2016). A review of recent advances in research on extreme heat events. *Current Climate Change Reports*, 2(4), 242–259. <https://doi.org/10.1007/s40641-016-0042-x>
- Hoskins, B. J., & Karoly, D. J. (1981). The steady linear response of a spherical atmosphere to thermal and orographic forcing. *Journal of Atmospheric Sciences*, 38(6), 1179–1196. [https://doi.org/10.1175/1520-0469\(1981\)038%3C1179:TSLROA%3E2.0.CO;2](https://doi.org/10.1175/1520-0469(1981)038%3C1179:TSLROA%3E2.0.CO;2)
- Im, E.-S., Pal, J. S., & Eltahir, E. A. B. (2017). Deadly heat waves projected in the densely populated agricultural regions of South Asia. *Science Advances*, 3(8), e1603322. <https://doi.org/10.1126/sciadv.1603322>
- Jones, R. H., Westra, S., & Sharma, A. (2010). Observed relationships between extreme sub-daily precipitation, surface temperature, and relative humidity. *Geophysical Research Letters*, 37, L22805. <https://doi.org/10.1029/2010GL045081>
- Kalkstein, L. S., & Davis, R. E. (1989). Weather and human mortality: An evaluation of demographic and interregional responses in the United States. *Annals of the Association of American Geographers*, 79(1), 44–64. <https://doi.org/10.1111/j.1467-8306.1989.tb00249.x>

- Kalkstein, L. S., & Valimont, K. M. (1986). An evaluation of summer discomfort in the United States using a relative climatological index. *Bulletin of the American Meteorological Society*, 67(7), 842–848. [https://doi.org/10.1175/1520-0477\(1986\)067%3C0842:AEOSDI%3E2.0.CO;2](https://doi.org/10.1175/1520-0477(1986)067%3C0842:AEOSDI%3E2.0.CO;2)
- Kanamitsu, M., Ebisuzaki, W., Woollen, J., Yang, S.-K., Hnilo, J. J., Fiorino, M., & Potter, G. L. (2002). NCEP–DOE AMIP-II Reanalysis (R-2). *Bulletin of the American Meteorological Society*, 83(11), 1631–1643. <https://doi.org/10.1175/BAMS-83-11-1631>
- Kennedy, A. D., Dong, X., Xi, B., Xie, S., Zhang, Y., & Chen, J. (2011). A comparison of MERRA and NARR reanalyses with the DOE ARM SGP data. *Journal of Climate*, 24(17), 4541–4557. <https://doi.org/10.1175/2011jcli3978.1>
- Knutson, T. R., & Ploshay, J. J. (2016). Detection of anthropogenic influence on a summertime heat stress index. *Climatic Change*, 138(1–2), 25–39. <https://doi.org/10.1007/s10584-016-1708-z>
- Kunkel, K. E., Changnon, S. A., Reinke, B. C., & Arlt, R. W. (1996). The July 1995 heat wave in the Midwest: A climatic perspective and critical weather factors. *Bulletin of the American Meteorological Society*, 77(7), 1507–1518. [https://doi.org/10.1175/1520-0477\(1996\)077%3C1507:TJHWIT%3E2.0.CO;2](https://doi.org/10.1175/1520-0477(1996)077%3C1507:TJHWIT%3E2.0.CO;2)
- Laîné, A., Nakamura, H., Nishii, K., & Miyasaka, T. (2014). A diagnostic study of future evaporation changes projected in CMIP5 climate models. *Climate Dynamics*, 42(9–10), 2745–2761. <https://doi.org/10.1007/s00382-014-2087-7>
- Lau, N.-C., & Nath, M. J. (2012). A model study of heat waves over North America: Meteorological aspects and projections for the twenty-first century. *Journal of Climate*, 25(14), 4761–4784. <https://doi.org/10.1175/JCLI-D-11-00575.1>
- Lee, Y.-Y., & Grotjahn, R. (2016). California Central Valley summer heat waves form two ways. *Journal of Climate*, 29(3), 1201–1217. <https://doi.org/10.1175/jcli-d-15-0270.1>
- Loikith, P. C., & Broccoli, A. J. (2012). Characteristics of observed atmospheric circulation patterns associated with temperature extremes over North America. *Journal of Climate*, 25(20), 7266–7281. <https://doi.org/10.1175/JCLI-D-11-00709.1>
- Lorenz, R., Jaeger, E. B., & Seneviratne, S. I. (2010). Persistence of heat waves and its link to soil moisture memory. *Geophysical Research Letters*, 37, L09703. <https://doi.org/10.1029/2010GL042764>
- Maddox, R. A., McCullum, D. M., & Howard, K. W. (1995). Large-scale patterns associated with severe summertime thunderstorms over central Arizona. *Weather and Forecasting*, 10(4), 763–778. [https://doi.org/10.1175/1520-0434\(1995\)010%3C0763:LSPAWS%3E2.0.CO;2](https://doi.org/10.1175/1520-0434(1995)010%3C0763:LSPAWS%3E2.0.CO;2)
- Mantua, N. J., & Hare, S. R. (2002). The Pacific Decadal Oscillation. *Journal of Oceanography*, 58(1), 35–44. <https://doi.org/10.1023/a:1015820616384>
- McKinnon, K. A., Rhines, A., Tingley, M. P., & Huybers, P. (2016). Long-lead predictions of eastern United States hot days from Pacific sea surface temperatures. *Nature Geoscience*, 9(5), 389–394. <https://doi.org/10.1038/ngeo2687>
- Melillo, J. M., Richmond, T. C., & Yohe, G. W. (Eds.) (2014). *Climate change impacts in the United States: The third national climate assessment*. U.S. Global Change Research Program (841 pp.). Washington, DC: U.S. Government Printing Office. <https://doi.org/10.7930/J0Z31WJ2>
- Mesinger, F., DiMego, G., Kalnay, E., Mitchell, K., Shafran, P. C., Ebisuzaki, W., ... Shi, W. (2006). North American Regional Reanalysis. *Bulletin of the American Meteorological Society*, 87(3), 343–360. <https://doi.org/10.1175/BAMS-87-3-343>
- Miralles, D. G., Teuling, A. J., van Heerwaarden, C. C., & de Arellano, J. V.-G. (2014). Mega-heatwave temperatures due to combined soil desiccation and atmospheric heat accumulation. *Nature Geoscience*, 7(5), 345–349. <https://doi.org/10.1038/ngeo2141>
- Mora, C., Dousset, B., Caldwell, I. R., Powell, F. E., Geronimo, R. C., Bielecki, C. R., ... Trauernicht, C. (2017). Global risk of deadly heat. *Nature Climate Change*, 7(7), 501–506. <https://doi.org/10.1038/nclimate3322>
- Mueller, N. D., Butler, E. E., McKinnon, K. A., Rhines, A., Tingley, M., Holbrook, N. M., & Huybers, P. (2015). Cooling of US Midwest summer temperature extremes from cropland intensification. *Nature Climate Change*, 6(3), 317–322. <https://doi.org/10.1038/nclimate2825>
- Nakamura, N., & Oort, A. H. (1988). Atmospheric heat budgets of the polar regions. *Journal of Geophysical Research*, 93(D8), 9510–9524.
- Ning, L., Riddle, E. E., & Bradley, R. S. (2015). Projected changes in climate extremes over the northeastern United States. *Journal of Climate*, 28(8), 3289–3310. <https://doi.org/10.1175/JCLI-D-14-00150.1>
- Pal, J. S., & Eltahir, E. A. B. (2016). Future temperature in southwest Asia projected to exceed a threshold for human adaptability. *Nature Climate Change*. <https://doi.org/10.1038/nclimate2833>
- Perkins, S. E. (2015). A review on the scientific understanding of heatwaves—Their measurement, driving mechanisms, and changes at the global scale. *Atmospheric Research*, 164–165, 242–267. <https://doi.org/10.1016/j.atmosres.2015.05.0140169>
- Pielke, R. A., Davey, C., & Morgan, J. (2004). Assessing “global warming” with surface heat content. *Eos*, 85(21), 210–211. <https://doi.org/10.1029/2004EO210004>
- Reynolds, R. W., Rayner, N. A., Smith, T. M., Stokes, D. C., & Wang, W. (2002). An improved in situ and satellite SST analysis for climate. *Journal of Climate*, 15(13), 1609–1625. [https://doi.org/10.1175/1520-0442\(2002\)015%3C1609:ALISAS%3E2.0.CO;2](https://doi.org/10.1175/1520-0442(2002)015%3C1609:ALISAS%3E2.0.CO;2)
- Schär, C. (2016). The worst heat waves to come. *Nature Climate Change*, 6, 128–129. <https://doi.org/10.1038/nclimate2864>
- Sherwood, S. C., & Huber, M. (2010). An adaptability limit to climate change due to heat stress. *Proceedings of the National Academy of Sciences*, 107(21), 9552–9555. <https://doi.org/10.1073/pnas.0913352107>
- Smith, T. T., Zaitchik, B. F., & Gohlike, J. M. (2013). Heat waves in the United States: Definitions, patterns, and trends. *Climatic Change*, 118(3–4), 811–825. <https://doi.org/10.1007/s10584-012-0659-2>
- Stull, R. (2011). Wet-bulb temperature from relative humidity and air temperature. *Journal of Applied Meteorology and Climatology*, 50(11), 2267–2269. <https://doi.org/10.1175/JAMC-D-11-0143.1>
- Teng, H., & Branstator, G. (2017). Causes of extreme ridges that induce California droughts. *Journal of Climate*, 30(4), 1477–1492. <https://doi.org/10.1175/jcli-d-16-0524.1>
- Teng, H., Branstator, G., Meehl, G. A., & Washington, W. M. (2016). Projected intensification of subseasonal temperature variability and heat waves in the Great Plains. *Geophysical Research Letters*, 43(5), 2165–2173. <https://doi.org/10.1002/2015gl067574>
- Teng, H., Branstator, G., Wang, H., Meehl, G. A., & Washington, W. M. (2013). Probability of US heat waves affected by a subseasonal planetary wave pattern. *Nature Geoscience*, 6, 1056–1061. <https://doi.org/10.1038/ngeo1988>
- Trenberth, K. E., Fasullo, J. T., & Mackaro, J. (2011). Atmospheric moisture transports from ocean to land and global energy flows in reanalyses. *Journal of Climate*, 24(18), 4907–4924. <https://doi.org/10.1175/2011jcli4171.1>
- Trenberth, K. E., & Guillemot, C. J. (1996). Physical processes involved in the 1988 drought and 1993 floods in North America. *Journal of Climate*, 9(6), 1288–1298. [https://doi.org/10.1175/1520-0442\(1996\)009%3C1288:PPITD%3E2.0.CO;2](https://doi.org/10.1175/1520-0442(1996)009%3C1288:PPITD%3E2.0.CO;2)
- Vincent, L. A., van Wijngaarden, W. A., & Hopkinson, R. (2007). Surface temperature and humidity trends in Canada for 1953–2005. *Journal of Climate*, 20(20), 5100–5113. <https://doi.org/10.1175/jcli4293.1>
- Wang, H., & Schubert, S. (2014). Causes of the extreme dry conditions over California during early 2013. *Bulletin of the American Meteorological Society*, 95(9). Supplement: Explaining extreme events of 2013 from a climate perspective

- Weaver, S. J., Schubert, S., & Wang, H. (2009). Warm season variations in the low-level circulation and precipitation over the central United States in observations, AMIP simulations, and idealized SST experiments. *Journal of Climate*, 22(20), 5401–5420. <https://doi.org/10.1175/2009jcli2984.1>
- Willett, K. M., & Sherwood, S. C. (2012). Exceedance of heat index thresholds for 15 regions under a warming climate using the wet-bulb globe temperature. *International Journal of Climatology*, 32(2), 161–177. <https://doi.org/10.1002/joc.2257>
- Wu, J., Zhou, Y., Gao, Y., Fu, J. S., Johnson, B. A., Huang, C., ... Liu, Y. (2014). Estimation and uncertainty analysis of impacts of future heat waves on mortality in the eastern United States. *Environmental Health Perspectives*, 122(1), 10–16. <https://doi.org/10.1289/ehp.1306670>
- Wuebbles, D., Meehl, G., Hayhoe, K., Karl, T. R., Kunkel, K., Santer, B., ... Sun, L. (2015). CMIP5 climate model analyses: Climate extremes in the United States. *Bulletin of the American Meteorological Society*, 95(4), 571–583. <https://doi.org/10.1175/bams-d-12-00172.1>